Prediction on the onset of global failure of irregular honeycombs under compression

†Youming Chen, Raj Das, and Mark Battley

Centre for Advanced composite materials, Department of Mechanical Engineering, University of Auckland, Auckland, New Zealand.

†Corresponding author: cyou659@aucklanduni.ac.nz

Abstract

In the present study, two irregular honeycombs are manufactured by a 3D printer and tested under compression. Experimental observation shows that the first fracture of cell walls is significantly critical, which is indeed the onset of global failure of honeycombs. To predict the onset of global failure of honeycombs, failure criteria based on stress or strain at integration point level need to be used, which is difficult to realize due to stress singularity at cell wall joints. To circumvent this issue, a mesh level, 40 elements within each cell wall, is chosen in FE analysis so that numerical results at cell wall joints are close to engineering solutions. Failure criteria based on von Mises stress, equivalent plastic strain, tensile plastic strain, surface tensile stress and bending moment are then employed to predict the first fracture of cell walls. It is found that failure criteria based on von Mises stress, equivalent plastic strain, tensile plastic strain yield the same predictions which are within 9% of experiment value for strength and within 24% for strain at failure. The cell walls which are predicted to be the most likely to fracture first in the honeycombs agree well with these cell walls that rupture first in experiments.

Keywords: Irregular honeycombs, fracture and failure, FE modelling

Introduction

As manufacturing techniques advance, cellular solids have seen a wide range of applications in automotive, aerospace, aircraft, marine, construction and packaging industries due to their advantage in weight-saving, impact-absorbing, thermal-insulating, noise-abating and so forth. Naturally, the mechanics of cellular solids have become a field of interest for researchers over the past few decades (a comprehensive review can be found in [Gibson and Ashby (1997)].

For the safe and efficient use of cellular solids, characterization of mechanical properties of cellular solids is vitally important and has been carried out extensively [Deshpande and Fleck (2000); Deshpande and Fleck (2001); Motz and Pippan (2001); Kabir, Saha et al. (2006); Daniel and Cho (2011); Battley, Clark et al. (2013)]. With tests under different loading conditions, the constitutive relations of cellular solids can be established [Deshpande and Fleck (2000); Deshpande and Fleck (2001)], which, however, are generally valid for a specific cellular solid. Generalization of constitutive relations of cellular solids can be found in [Gibson and Ashby (1997)]. To develop tools of predicting the properties of cellular solids, cellular solid modelling have been progressed from simple single cell models [Gibson and Ashby (1982)] to complicated models of random geometry [Ribeiro-Ayeh (2005); Chen, Das et al. (2014)]. Through modelling, it is recognized that the global response of cellular solids is strongly related to their relative density, microstructure and the properties of base materials [Gibson, Ashby et al. (1982); Gibson and Ashby (1982); Ribeiro-Ayeh (2005); Chen, Das et al. (2014)].

The majority of modelling work has been undertaken to study the elastic response of cellular solids [Zhu, Knott et al. (1997); Grenestedt and Tanaka (1998); Simone and Gibson (1998); Simone and Gibson (1998); Grenestedt and Bassinet (2000); Roberts and Garboczi (2001); Gan, Chen et al. (2005); Ribeiro-Ayeh (2005); Li, Gao et al. (2006); Chen, Das et al. (2014)]. In terms of instability analysis of cellular solids which involves geometrical and material nonlinearity, limited work has been conducted. Papka and Kyriakides [Papka and Kyriakides (1994); Papka and Kyriakides (1998)] numerically reproduced the crushing process of aluminum hexagonal honeycombs with integration of geometric imperfections. Zhu etc. [Zhu, Thorpe et al. (2006)] studied the effect of cell irregularity on the high strain compression of Voroni honeycombs using Abaqus Riks method.

In their models cell wall material was assumed to be elastic, therefore the typical stress plateau of honeycombs under compression did not occur and the nonlinearity of response of Voroni honeycombs under high strain arises solely from large deformation of cell walls. Jouneid and Sab. [Jouneid and Sab (2009)] pointed out global buckling (a great number of cell walls buckle simultaneously) disappear in irregular honeycombs, and thus elastic buckling analysis is not able to predict the instability of irregular honeycombs. Kyriakides etc. [Jang, Kyriakides et al. (2010); Gaitanaros, Kyriakides et al. (2012)] simulated the crushing of an open-cell aluminum foam using LS-DYNA. The typical three stages: initial elastic, stress plateau and densification regimes were reproduced. It is noteworthy that the spread of localized band of crushed cells agrees well with experimental observation made using X-ray tomography. Nammi ect. [Nammi, Myler et al. (2010)] modelled the compressive response of a closed-cell aluminum foam using a repeating unit cell constructed from the tetrakaidecahedra structure, and remarkable stress fluctuation in stress plateau regime were predicted. Daxner and Bische [Robert (2005); Daxner, Bitsche et al. (2006); Daxner (2010)] predicted the yield surface of Kelvein and Weaire-Phelan closed-cell foams using macroscopic plastic effective strain and energy dissipated as criteria to define the onset of global failure of foams. Mills [Mills (2010)] investigated the yield surface of polyethylene and polystyrene closed-cell foams using the Kelvin foam model, with foam failure defined by the moment when the yield zone (equivalent plastic strain larger than 0.01) crosses the foam structure.

In above mentioned simulations, cell wall materials are assumed to be elastic-plastic (except [Zhu, Thorpe et al. (2006); Jouneid and Sab (2009)], without consideration of material fracture. This is valid for cellular solids made from ductile material such as aluminum subjected to compression, because no cell wall fracture was experimentally observed during compressive tests. However, for these cellular solids made from brittle or quasi-brittle materials, cell walls fracture at some stage, leading to the failure of cellular solids. Additionally, when cellular solids are subjected to tension or shear, they fail by cell walls tearing apart. Therefore, material failure criteria need to be incorporated into models to predict the failure of cellular solids. To apply material failure criteria, accurate stress or strain (Von Miss stress or equivalent plastic strain) at integration point should be used. However, due to stress singularity at the corners of cells (cell wall joints), stress and strain are actually mesh dependent. Hence, appropriate mesh size should be determined and adopted.

Due to three dimensionality, it is difficult to observe the deformation and failure pattern at cell wall level in foams, and thus is challenging to validate foam models. Honeycombs, as a member of the family of cellular solids, are often employed to study the mechanics of cellular solids due to their geometric simplicity [Papka and Kyriakides (1994); Papka and Kyriakides (1998)]. The deformation of each cell wall in honeycombs can be readily captured by camera and used to validate numerical models [Papka and Kyriakides (1994)]. Nevertheless, in most of cellular solids, variations in microstructures are ubiquitous, for instance, irregular cell shape, non-uniform cell size and wall thickness. Therefore, irregular honeycombs, such as honeycombs with random wall thickness and cell size, are more geometrically representative of realist cellular solids. It is a challenging task to manufacture irregular honeycombs in conventional manner, but with 3D printing it become easier.

This paper aims to predict the onset of global failure of irregular honeycombs under compression which fail by cell wall fracture. To accomplish this, two irregular honeycombs are manufactured by a 3D printer and tested under compression firstly. During the tests, progressive cell wall fracture is captured by a camera positioned squarely toward the specimens. The mechanical properties of base material of the honeycombs are measured with printed dogbone specimens and subsequently incorporated into finite element (FE) models. Static analyses are conducted in Abaqus for these two honeycombs. Then different failure criteria are utilized to predict the onset of global failure of the honeycombs, and finally these predictions are compared.

Experiments

In the present study specimens were manufactured by a 3D printer (Projet HD 3500 Plus), which has a net build volume of 203 × 178 × 152 mm. The build material VisiJet M3 X is utilized. The highest printer resolution of 16 μm layers (750x750x1600 DPI (xyz)) was chosen. As 3D printers build parts by stacking a layer of materials on top of the previous layer, the properties of printed materials may be anisotropic and different from that of raw materials, and thus the properties of the printed materials still need to be measured. To this end, dogbone specimens of type I were printed in three orthogonal orientations (see Figure 1a) and tensile tests were conducted with them.

Two irregular honeycombs of uniform wall thickness but having cell size (diameter of incircle of cells) following prescribed log-normal distributions (see Figure 1b) were printed here. To print these specimens, the geometry need be created first, which is done in the software Abaqus using python scripts. Firstly, a precursor honeycomb without wall thickness (dashed line in Figure 2) is created, which is indeed a 2D Laguerre tessellation. The details of the generation of 2D Laguerre tessellations are given in [Chen, Das et al. (2014)]. Once the precursor honeycomb is generated, the points, lines, and cells are labelled and stored in a hierarchical order, so that the topologies can be readily known, i.e., which lines construct a cell and which points form a line. Thereafter, cell wall thickening is performed for all the cells one by one. To illustrate the thickening process, we take a cell ABCDE (see Figure 2) as an example. First we determine the inner normal of each edge of the cell ABCDE. As the thickness of each wall is given, five linear equations which represent lines coincidental with inner edges (A'B', B'C', C'D', D'E' and E'A') can be developed. Solving a set of two linear equations which represent two adjoining inner edges can yield the coordinates of an inner vertex, such as A'. Following the same process by rotation, the coordinates of the other four inner vertices (B', C', D', E') are calculated. Each cell is analysed through this process, and then all the edges of cell walls are determined. With all the topological data obtained by this process, a sketch is drawn and extruded to 3D geometry in Abaqus. Two thin plates are added at two edges (see Figure 1b) to protect cell walls at edges from localized damage due to contact with compression platens.

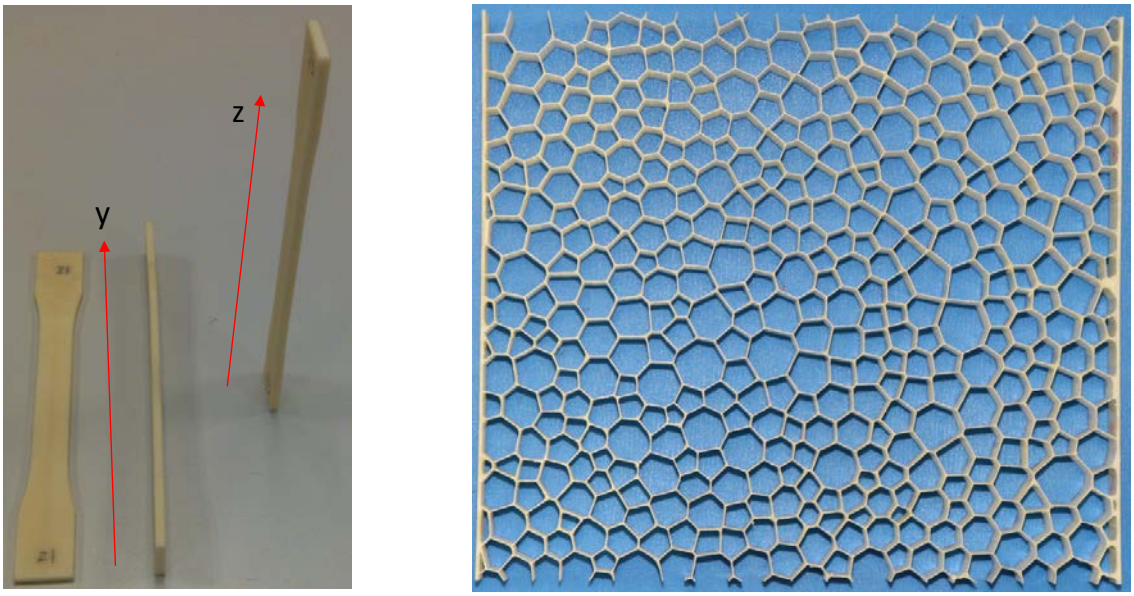

(a) (b)

Figure 1: (a) printing orientations of dogbone specimens; (b) printed regular honeycomb

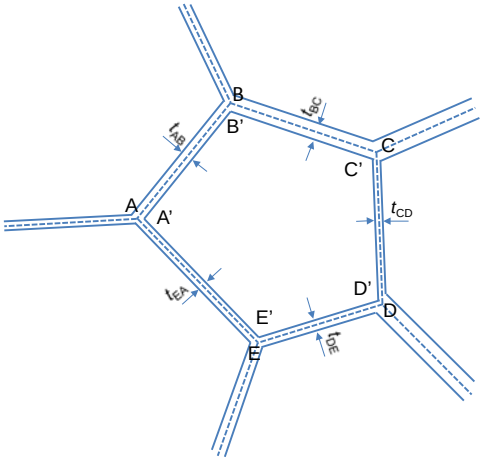

Figure 2: Schematics of cell wall thickening

As specimen size is limited by the maximum building volume of the 3D printer, the more the cells in the specimens are, the smaller the cell size is and the thinner the cell walls are, which make it difficult for the camera to capture deformation at cell wall level and for the 3D printer to print. Here the average cell size is chosen to be 4.46 mm, with a standard deviation of 1 mm, and cell wall thickness is set to be 0.3 mm. The specimens are 170 mm wide, 190 mm tall and 25 mm thick. Compressive tests were subsequently carried out with a synchronized camera positioned squarely toward the specimens to capture deformation in honeycombs.

Computational models

In modelling of compression of ductile honeycombs, it is not necessary to accurately calculate stress and strain at integration point level since the predicted global response is generally not sensitive to them. Nevertheless, it is critical for brittle honeycombs, because stress and strain at integration point level determine whether or not cell walls rupture and thus affect the prediction of global response of honeycombs. However, it is impossible to calculate the exact stress and strain at cell wall joints due to stress singularity. Engineering solutions are more effective and practical in predicting beam failure than exact solutions. For example, Davidge [Davidge (1979)] pointed out that brittle beams rupture when maximum surface tensile stress (σ_{max}) is 1.1 times the ultimate tensile strength of beam material, maximum surface tensile stress is calculated as

$$\sigma_{max} = \frac{6M_{max}}{bt^2} \tag{1}$$

where M_{max} is maximum bending moment, and b and t are the width and thickness of the beam, respectively. In a compressed honeycomb, cell walls are basically under the conditions similar to the beam shown in Figure 3a. If we adjust mesh size in FE analysis to make numerical results (surface stress and bending moment) match engineering solutions, then the numerical results at integration points can be utilized to determine cell walls fracture. To find out the mesh size, a mesh sensitivity study is conducted for the beam shown in Figure 3a. The beam is modeled using shell elements (S4R), with one element along width direction, as shown in Figure 3b. Beam material is assumed to be elastic. One end of the beam is fixed and the other is constrained from rotating and pushed downward a third of length of the beam. Three beam length-to-thickness ratios, 10, 20 and 30, are considered. The maximum surface stress and bending moment are read at the integration points. The engineering solutions for surface stress and bending moment are calculated by Eq. (1) and Eq. (2).

$$M_{max} = \frac{FL}{2} \tag{2}$$

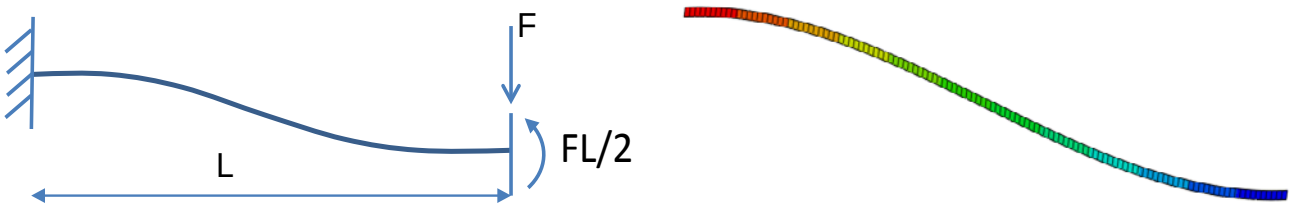

(a) (b)

Figure 3: (a) beam with one end fixed and one end constrained from rotating subjected to a load at the free end; (b) FE model of the beam

The honeycombs are modelled by shell element (S4R) as well. The geometry of shell models is extruded from the precursor sketches mentioned in the experiments section. Instead of full model, the compression of honeycombs is seen as plain strain and thus only a slice of honeycomb (0.5 mm thick) is modelled, with one element along thickness direction. All elements are constrained moving along honeycomb thickness direction. The tensile properties measured with printed dogbone are incorporated into models. Since the simulations is up to the point when cell wall start to break and no cell wall contact occurs before that, static analyses with large deformation considered are conducted.

Results and discussion

In this section, the tensile properties measured with dogbone specimens are presented firstly. Then the compressive response of the honeycombs is described. The results of mesh study are subsequently illustrated. Finally, the predictions on the onset of honeycomb failure with different criteria are developed and discussed.

Experimental results

Table 1 lists the measured modulus, ultimate tensile strength and elongation at break of material printed in different orientations. It can be seen that the printed specimens give Young's modulus reasonably closed to that of raw material. The ultimate stresses of the specimens printed standing up along y direction and lying along y direction are slightly smaller than that of raw material, while the specimens printed along z direction exhibit ultimate stress 35.5% lower than that of raw material, which is attributable to the way of 3D printer making part by stacking materials. As honeycombs are built up along thickness direction, the properties measured with specimens printed standing up along Y direction, as shown in Figure 4, is adopted in numerical models.

Table 1. Measured properties of printed dogbone specimens

	Modulus (Chord 0.05%-0.25%) (GPa)	Ultimate tensile strength (MPa)	Elongation at break (standard) (%)
Lying along Y direction	2.05 ± 0.06	44.3 ± 0.36	3.98 ± 0.07
Standing up along Y direction	2.34 ± 0.03	45.9 ± 0.36	5.71 ± 0.42
Z direction	2.27 ± 0.03	31.6 ± 2.57	1.98 ± 0.30
Raw material	2.17	49.0	8.3

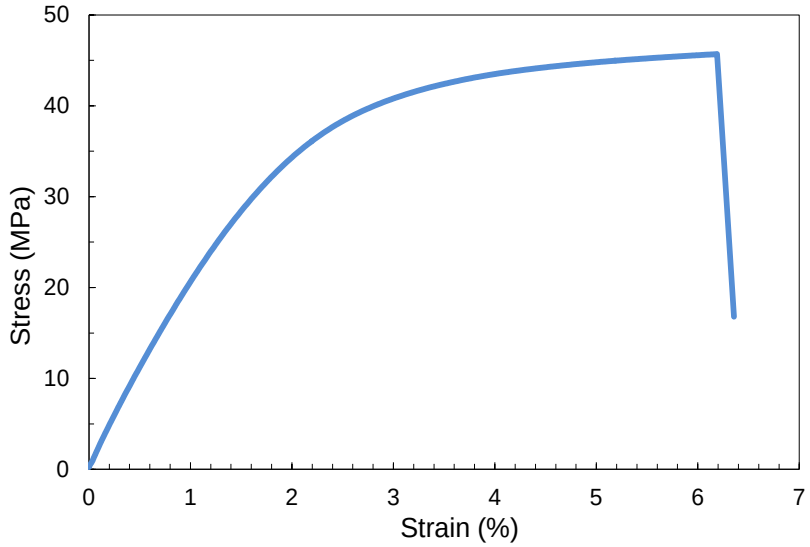

Figure 4: Stress-strain curve of the dogbone specimens printed standing up along Y direction

During the compression, it was observed that cell walls fracture progressively. Figure 5 shows the compressive stress-strain of the two irregular honeycombs. Each drop in stress in Figure 5 corresponds to one or multiple cell wall fracture. The first fracture of cell wall occurs at a strain of 0.078 (marked as point A in Figure 5) for specimen-1 and at a strain of 0.071 (marked as point A in Figure 5) for specimen-2, giving failure stresses 40.6 kPa and 33.3 kPa, respectively. It is noteworthy that the first fracture of cell walls are important as it marks the onset of global failure of honeycombs. The configurations of specimen-1 and specimen-2 corresponding to point A and B are shown in Figure 6, and the cell walls that rupture at the moment are marked by a line.

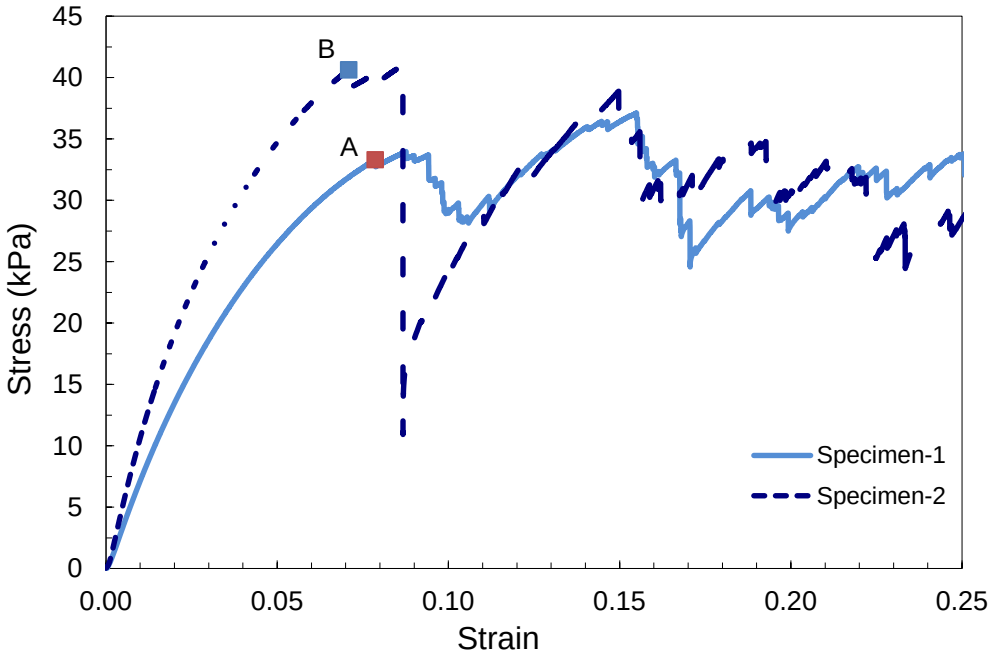

Figure 5: Compressive stress-strain curves of the honeycombs

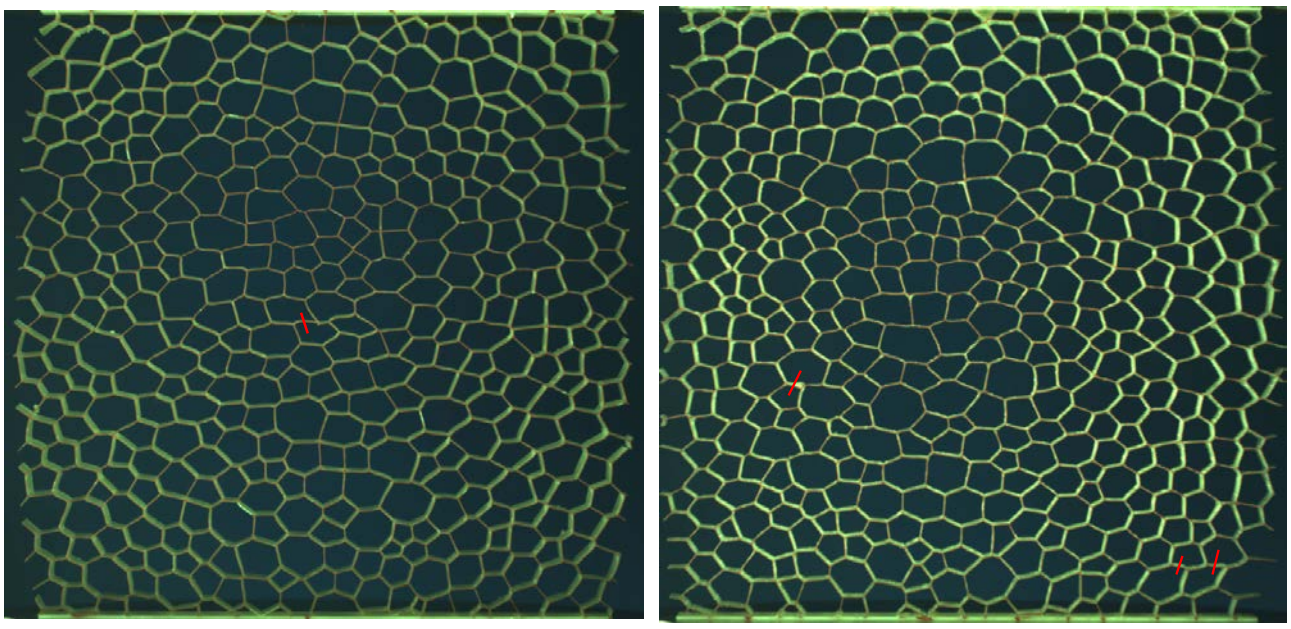

(a) (b)

Figure 6: Configurations of specimens: (a) specimen-1;(b) specimens 2 at the point when the first fracture of cell walls occurs

Numerical results

As to the mesh sensitivity study with the beam shown in Figure 3a, the maximum surface tensile stress and bending moment at the fixed end obtained by FE analysis are compared against engineering solutions here. Figure 7 shows the variation of ratio of numerical results to engineering solutions with element number in the beam. The ratio increases with increasing element number. With 40 elements, numerical results are 97.5% of engineering solutions. Additionally, it is found that the variation of this ratio with element number is insensitive to beam configuration (thickness-

length ratio). Considering computational cost and accuracy, the mesh level of 40 elements within each cell wall is chosen in the subsequent honeycomb simulations.

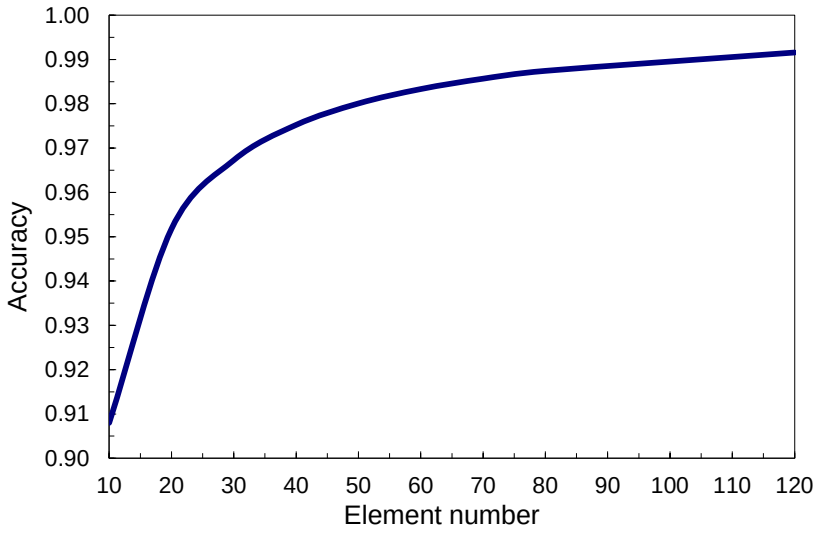

Figure 7: Variation of accuracy of stress prediction at the ends of the beam with element number

Figure 8 shows the comparison of compressive stress-strain curves of honeycombs between experiments and FE analysis. It can be seen that for specimen-2, the predicted stress-strain curve agrees well with experimental counterpart before the first fracture of cell wall (point B), while the predicted stress for specimen-1 is a little larger than experimental value, which could be attributable to imperfections induced during manufacturing.

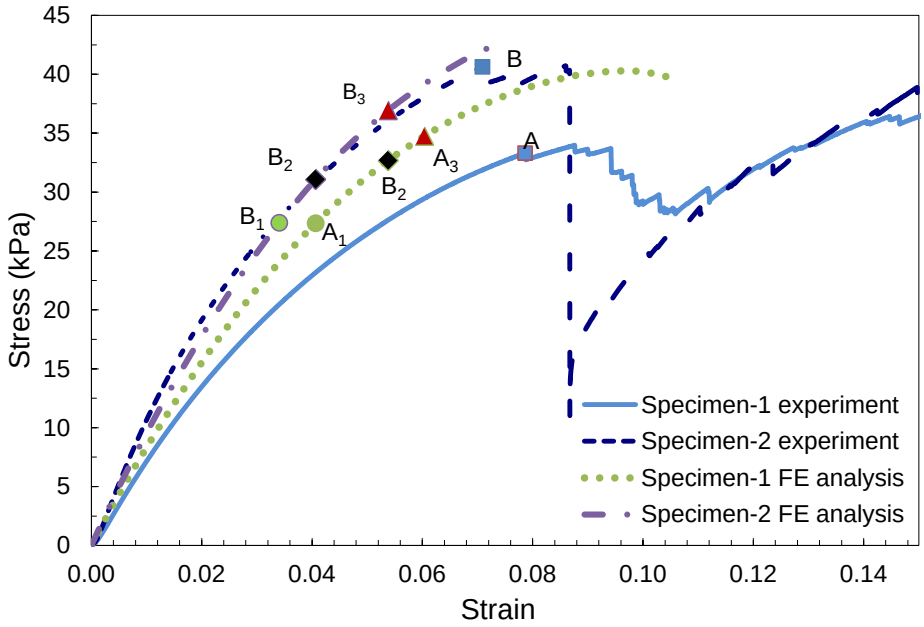

Figure 8: Comparison of stress-strain curve between experiments and FE analysis

To predict the first fracture of cell walls, criteria based on tensile stress, bending moment, von Mises stress, tensile plastic strain and equivalent plastic strain are used. When tensile stress, bending moment, von Mises stress, tensile plastic strain and equivalent plastic strain at an integration point of a cell wall reach specified values, the cell wall fracture and the honeycomb fails. In order to establish failure criteria, the data from tensile tests with printed dogbone are

employed there, namely, ultimate stress (45.9 kPa) and plastic strain (0.04) at breaking point. All the criteria are listed in Table 2. For bending moment criterion, as mentioned in the computational model section, 1.1 times the ultimate tensile stress are used, and bending moment here is actually bending moment force per unit width. With these criteria, The onset of failure of honeycombs are predicted and marked in Figure 8, with points A_1 and B_1 by bending moment criterion, points A_2 and B_2 by tensile stress criterion and points A_3 and B_3 by von Mises stress, equivalent plastic strain and tensile plastic strain criteria. The corresponding strength and strain at failure of the honeycombs are listed in Table 2. It is noticeable that criteria based on von Mises stress, equivalent plastic strain and tensile plastic strain yield the same results, which are the closest to experimental results, within 9% for strength and within 24% for strain at failure. Figure 9 shows all the cell walls which have maximum von Mises stress larger than 45 at the point of honeycomb failure. These cell walls are the most vulnerable and have the greatest potential to fracture first in the honeycombs, which agree well with the cell walls that fracture first in experiments.

Table 2. Strength and strain at failure of the honeycombs predicted by different criteria

Variables	Criteria	Predicted strength (kpa)		Predicted strain at failure	
		Specimen-1	Specimen-2	Specimen-1	Specimen-2
Tensile stress (σ_{max}) (kPa)	σ_{max}=45.9	32.7	31.1	0.054	0.041
Bending moment (M_{max}) (N)	$M_{max=}45.9\times1.1\times0.3^2/6$	27.4	27.4	0.041	0.034
von Mises stress (σ_{mises}) (kPa)	σ_{mises}=45.9	34.8	36.9	0.060	0.054
Tensile plastic strain (ε_p)	ε_p=0.4	34.8	36.9	0.060	0.054
Equivalent plastic strain (ε_{pe})	ε_{pe}=0.4	34.8	36.9	0.060	0.054
Experimental results		33.3	40.6	0.078	0.071

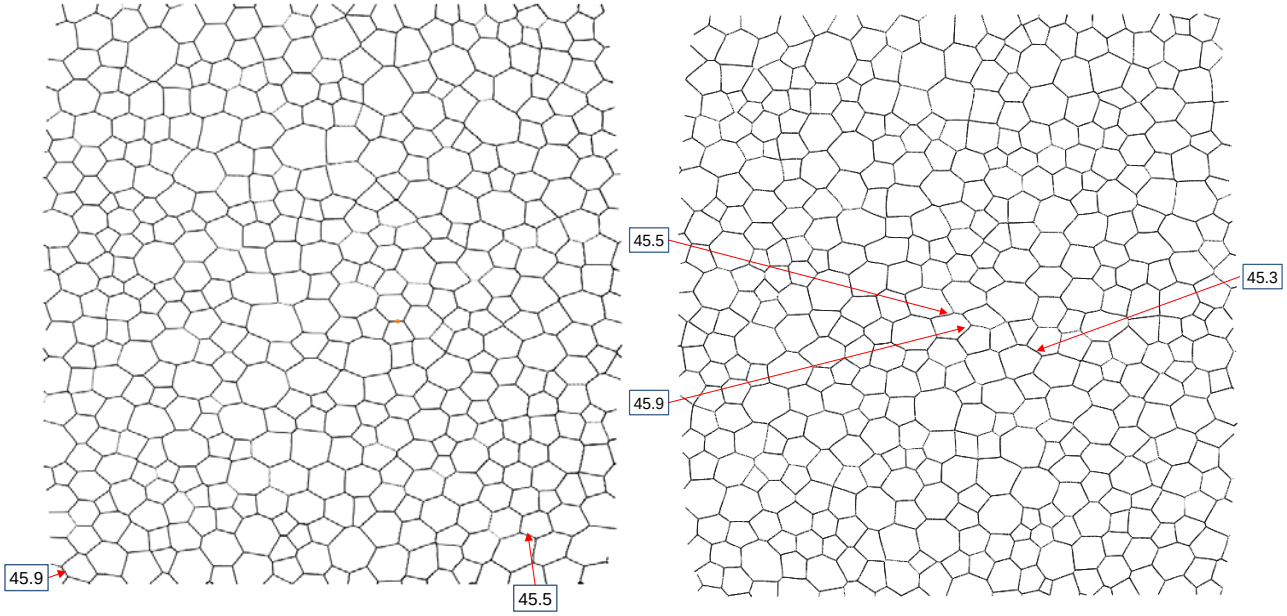

(a) (b)

Figure 9: Configurations of (a) specimen-1; (b) specimen-2 at failure point in FE analysis and cell walls which may fracture first

Conclusions

This paper concerns with predicting the onset of failure of irregular honeycombs. Due to stress singularity, the exact stress and strain at cell wall joints cannot be calculated. To circumvent this issue, a mesh level with 40 elements within each cell wall is adopted in FE models so that the calculated stress and strain at cell wall joints are close to engineering solutions. Then tensile stress, plastic strain, bending moment, von Mises stress and equivalent plastic strain at integration point level are used to predict the global failure of honeycombs. It is found that criteria based on von Mises stress, equivalent plastic strain and tensile plastic strain give the same predictions, which are the closest to experimental values, within 9% for strength and within 24% for strain at failure. The cell walls which are predicted to have the greatest potential to fracture first in the honeycombs agree well with these cell walls that rupture first in experiments. In summary, with a mesh level of 40 elements in each cell wall and von Mises stress, equivalent plastic strain and tensile plastic strain criteria, the onset of global failure of brittle honeycombs can be reasonably predicted. However, the deviation of predicted strain at failure from experiment value is not negligible. More specimens will be printed and tested in the future to further confirm the modelling.

References

Battley, M. A., A. M. Clark, et al. (2013). "Shear strength of sandwich core materials subjected to loading rates relevant to water slamming." Journal of Reinforced Plastics and Composites: 0731684413509424.

Chen, Y., R. Das, et al. (2014). "Effects of cell size and cell wall thickness variations on the stiffness of closed-cell foams." International Journal of Solids and Structures.

Daniel, I. and J.-M. Cho (2011). "Characterization of anisotropic polymeric foam under static and dynamic loading." Experimental mechanics **51**(8): 1395-1403.

Davidge, R. W. (1979). Mechanical behaviour of ceramics, CUP Archive.

Daxner, T. (2010). Finite element modeling of cellular materials. Cellular and Porous Materials in Structures and Processes, Springer**:** 47-106.

Daxner, T., R. D. Bitsche, et al. (2006). "Space-filling polyhedra as mechanical models for solidified dry foams." Materials Transactions **47**(9): 2213.

Deshpande, V. and N. Fleck (2001). "Multi-axial yield behaviour of polymer foams." Acta Materialia **49**(10): 1859-1866.

Deshpande, V. S. and N. A. Fleck (2000). "High strain rate compressive behaviour of aluminium alloy foams." International Journal of Impact Engineering **24**(3): 277-298.

Deshpande, V. S. and N. A. Fleck (2000). "Isotropic constitutive models for metallic foams." Journal of the Mechanics and Physics of Solids **48**(6–7): 1253-1283.

Gaitanaros, S., S. Kyriakides, et al. (2012). "On the crushing response of random open-cell foams." International Journal of Solids and Structures **49**(19–20): 2733-2743.

Gan, Y. X., C. Chen, et al. (2005). "Three-dimensional modeling of the mechanical property of linearly elastic open cell foams." International Journal of Solids and Structures **42**(26): 6628-6642.

Gibson, L., M. Ashby, et al. (1982). "The mechanics of two-dimensional cellular materials." Proceedings of the Royal Society of London. A. Mathematical and Physical Sciences **382**(1782): 25-42.

Gibson, L. J. and M. Ashby (1982). "The mechanics of three-dimensional cellular materials." Proceedings of the Royal Society of London. A. Mathematical and Physical Sciences **382**(1782): 43-59.

Gibson, L. J. and M. F. Ashby (1997). Cellular solids : structure and properties. Cambridge ; New York, Cambridge University Press.

Grenestedt, J. L. and F. Bassinet (2000). "Influence of cell wall thickness variations on elastic stiffness of closed-cell cellular solids." International Journal of Mechanical Sciences **42**(7): 1327-1338.

Grenestedt, J. L. and K. Tanaka (1998). "Influence of cell shape variations on elastic stiffness of closed cell cellular solids." Scripta Materialia **40**(1): 71-77.

Jang, W. Y., S. Kyriakides, et al. (2010). "On the compressive strength of open-cell metal foams with Kelvin and random cell structures." International Journal of Solids and Structures **47**(21): 2872-2883.

Jouneid, F. and K. Sab (2009). Elastic Buckling of 2-D Random Honeycombs: Does a Representative Volume Element Exists? IUTAM Symposium on Mechanical Properties of Cellular Materials. H. Zhao and N. A. Fleck, Springer Netherlands. **12:** 77-86.

Kabir, M. E., M. C. Saha, et al. (2006). "Tensile and fracture behavior of polymer foams." Materials Science and Engineering: A **429**(1–2): 225-235.

Li, K., X. L. Gao, et al. (2006). "Effects of cell shape and strut cross-sectional area variations on the elastic properties of three-dimensional open-cell foams." Journal of the Mechanics and Physics of Solids **54**(4): 783-806.

Mills, N. (2010). "Deformation mechanisms and the yield surface of low-density, closed-cell polymer foams." Journal of Materials Science **45**(21): 5831-5843.

Motz, C. and R. Pippan (2001). "Deformation behaviour of closed-cell aluminium foams in tension." Acta Materialia **49**(13): 2463-2470.

Nammi, S., P. Myler, et al. (2010). "Finite element analysis of closed-cell aluminium foam under quasi-static loading." Materials & Design **31**(2): 712-722.

Papka, S. D. and S. Kyriakides (1994). "In-plane compressive response and crushing of honeycomb." Journal of the Mechanics and Physics of Solids **42**(10): 1499-1532.

Papka, S. D. and S. Kyriakides (1998). "Experiments and full-scale numerical simulations of in-plane crushing of a honeycomb." Acta Materialia **46**(8): 2765-2776.

Ribeiro-Ayeh, S. (2005). Finite element modelling of the mechanics of solid foam materials, Karlstad University.

Robert, B. (2005). Space-filling polyhedra as mechanical models for solidified dry foams. PhD, Vienna University of Technology.

Roberts, A. P. and E. J. Garboczi (2001). "Elastic moduli of model random three-dimensional closed-cell cellular solids." Acta Materialia **49**(2): 189-197.

Simone, A. and L. Gibson (1998). "The effects of cell face curvature and corrugations on the stiffness and strength of metallic foams." Acta Materialia **46**(11): 3929-3935.

Simone, A. and L. Gibson (1998). "Effects of solid distribution on the stiffness and strength of metallic foams." Acta Materialia **46**(6): 2139-2150.

Zhu, H., J. Knott, et al. (1997). "Analysis of the elastic properties of open-cell foams with tetrakaidecahedral cells." Journal of the Mechanics and Physics of Solids **45**(3): 319-343.

Zhu, H. X., S. M. Thorpe, et al. (2006). "The effect of cell irregularity on the high strain compression of 2D Voronoi honeycombs." International Journal of Solids and Structures **43**(5): 1061-1078.